JOURNAL OF APPLIED ELECTROCHEMISTRY **27** (1997) 1193–1197

Thermal stability of electrodeposited Ni–P alloys

J.-P. BONINO, S. BRUET-HOTELLAZ, C. BORIES, P. POUDEROUX, A. ROUSSET

Laboratoire de Chimie des Matériaux Inorganiques, Université Paul Sabatier, 31062, Toulouse, France

Received 15 March 1996; revised 6 December 1996

Ni–P alloys were electrodeposited from phosphorous acid solutions in order to study their thermostructural stability, thermal desorption, and dimensional modifications during heat treatments. The quantity of phosphorus codeposited is not a linear function of the bath phosphorous acid content. X-ray diffraction shows that three characteristic composition ranges can be defined. In the first, corresponding to a Ni–P solid solution containing up to 9 at% of phosphorus, the microstructural refining is attended by a disappearance of the (1 0 0) preferential orientation. Simultaneously with this textural change, a slight adsorption of hydrogen is observed. Beyond 9 at% of phosphorus, the microcrystallized alloys are preferentially oriented in the [111] direction, and the gradual amorphization of Ni–P alloys is attended by adsorption of a very high volume of hydrogen. Beyond 17 at% of phosphorus, the alloys are amorphous and the amount of hydrogen included during the electrocrystallization is at its maximum. A large part of the hydrogen is desorbed before the crystallization temperature and less of it is desorbed during the crystallization.

1. Introduction

Ni–P alloys are well known for their good corrosion resistance and mechanical properties. It can be produced by electrodeposition, which also enables electroforming of thick amorphous or microcrystallized alloys. Although the metalloid codeposition process is influenced by experimental conditions (pH, temperature, additive, and current density) [1–4], Ni–P electrodeposits are generally brittle. It may be supposed that this brittleness is caused by atomic or molecular hydrogen inclusions in the deposits [5]. The atomic inclusion of nascent hydrogen H° would be expected to be highly mobile and combine to form molecular hydrogen (H_2). In an earlier paper [6], we added saccharin to Ni–P bath so to reduce the internal stresses of Ni–P deposits. But another method would be to desorb hydrogen from the coating by heat treatment at 100 °C for 1 h. Zeller [7] showed that, thermal desorption treatment decreases the ductility of $Ni_{80}P_{20}$ electrodeposits but a residual brittleness persists, apparently caused by voids observed within the deposit. In this paper, we correlate texture modifications of Ni–P coatings with phosphorus codeposition and hydrogen adsorption during amorphization. We use an analysis of the material thermal stability to show the effects of heat treatment on crystallization, desorption and dimensional modifications of alloys with various phosphorus contents.

2. Experimental conditions

Electrodeposited Ni–P alloys, about 40 μm thick were prepared from a phosphorous acid bath with nickel sulfate and chloride (Table 1). Electroplating was performed on etched flat copper substrate, in a plating cell with hydrodynamic flow parallel to the cathodic surface (Fig. 1). The anode was nickel sheet. The current density was 10 A dm^{-2}. After deposition, the copper substrate was removed by selective dissolution in a trichloroacetic and ammonia solutions.

Chemical composition was determined by atomic absorption spectrometry. Crystallite orientation was determined by X-ray diffraction using the K_α ray of cobalt ($\lambda = 0.179\,02$ nm).

The thermal stability of the material was determined by differential thermal analysis (DTA) in a nitrogen atmosphere with a 5 °C min^{-1} heating rate. To characterize the thermostructural variations by X-ray diffraction, each sample was heated in nitrogen for one hour at a temperature determined from the DTA curves. This analysis was complemented by thermal expansion analysis (TEA) of the dimensional stability during heat treament, in argon. For this TEA, the samples were made of parallelepipedic electroformed alloys and the heating rate was 5 °C min^{-1}. The thermodesorption of hydrogen was conducted by thermodesorption analysis (TDA) using a gaseous chromatomatography device. The heating rate was 10 °C min^{-1}.

3. Experimental results and discussion

3.1. *Chemical composition*

Electrodeposition of phosphorus from aqueous electrolyte on a cathode surface is possible only when the phosphorus is alloyed with another stable metal. Figure 2 shows that the addition of phosphorous acid to the bath makes it possible to codeposit phosphorus with nickel. The mechanism responsible for this simultaneous codeposition of nickel and phosphorus is poorly understood, but probably results from several direct and indirect reactions [2].

Table 1. Electrolyte composition and operating conditions

Component	*Content*
Composition	
$NiSO_4$, $7H_2O$	210 g dm^{-3}
$NiCl_2$, $6H_2O$	60 g dm^{-3}
Na_2SO_4	50 g dm^{-3}
H_3PO_4	50 g dm^{-3}
H_3PO_3	0 to 25 g dm^{-3}
Sodium lauryl sulfate	1 ml dm^{-3}
Conditions	
Temperature	80 °C
pH	2
Current density	10 A dm^{-2}
Agitation	N_2
Anode	Nickel

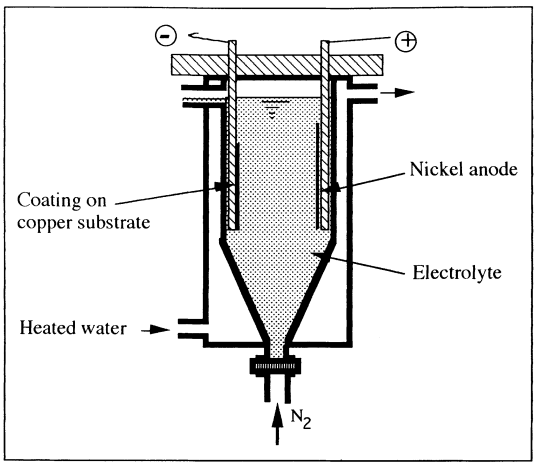

Fig. 1. Electroplating cell.

It can be seen in Fig. 2 that the phosphorus content in the deposits is not a linear function of the phosphorous acid concentration in the bath, but increases in two stages, apparently corresponding to a change in mechanism for codeposition of P with Ni for phosphorous acid concentrations above 7 g dm^{-3}. Figure 2 also shows that increases in codeposited phosphorus are attended by decreases in cathode current efficiency. For small additions of H_3PO_3 in the bath, we observe a strong increase in phosphorus content, which may be explained by a decrease in hydrogen surtension [8]. Beyond 5 at% of P, a first inflection appears in both curves, the current efficiency decreasing slowly while the increase in phosphorus content is attenuated. Between 7 and 12.5 g dm^{-3} of H_3PO_3 in the bath, the codeposition of phosphorus increases rapidly, reaching 17 at%. In this range, the current efficiency decreases from 0.75 to its minimum value of 0.60. From 12.5 to 25 g dm^{-3} H_3PO_3, the phosphorus content increases slowly to a saturation value of 22 at %.

As shown by the X-ray diffraction data in Fig. 3, inclusion of P in the Ni metal matrix significantly influences the electrocrystallization process. Although no crystallized nickel phosphide phase was detected, broadening of the nickel diffraction peaks with increasing phosphorus content indicates refining of deposit microstructure, apparently induced by phosphorus dissolved in a supersatured solid solution of nickel [9, 10]. Also, as P is added to the deposit, the (1 0 0) preferred orientation for the pure nickel decreases while the (1 1 1) increases slightly. This may be associated with differences in the degree of adsorbed hydrogen atoms on the (1 0 0) and (1 1 1) planes [11, 12]. Above 2 at% phosphorus, the (1 1 1) texture also decreases, the deposit becoming practically amorphous at phosphorous concentrations greater than about 14 at%. With the progressive transition from the microcrystallized to the amorphous state, between 2 and 14 at% of phosphorus, a shift of the (1 1 1) peak appears which can be attributed to a strong decrease in the interreticular distance of the (1 1 1) planes, as shown in Fig. 4. The widening of diffraction peaks is characteristic of structural disorder, but it can also result from microstresses in crystallites, while the shift of the (1 1 1) peak may result from macrostresses induced by adsorption of gaseous species. Since the variation of interreticular distance corresponds to the rapid decrease in current efficiency (Fig. 7), formation and inclusion of gaseous species H° or H_2 might be involved as Zeller had shown [7].

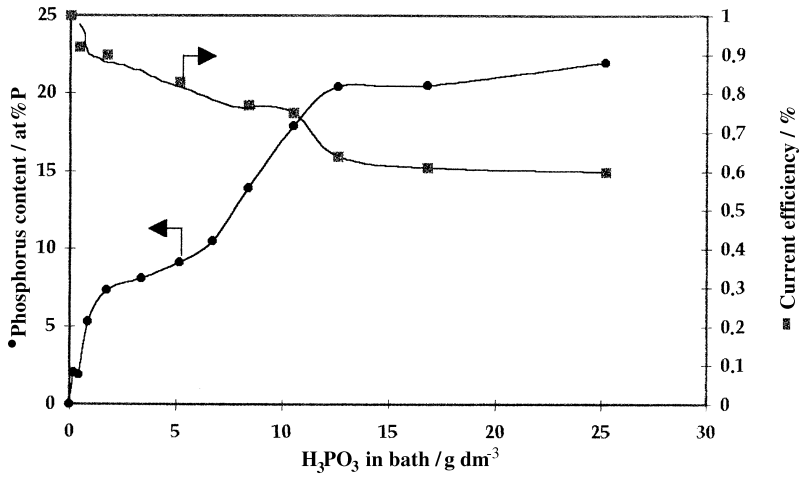

Fig. 2. Variation of phosphorus content and current efficiency against H_3PO_3 content in bath.

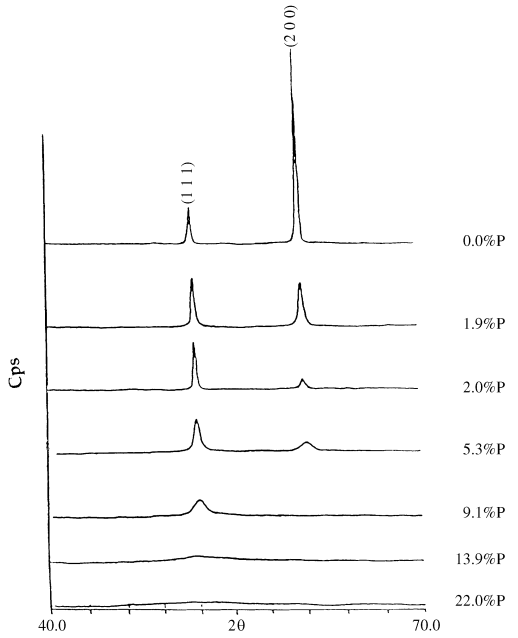

Fig. 3. Variation of X-ray diffraction patterns of Ni–P electrodeposits against phosphorus content in alloys. Obtained from θ–2θ diffractometer using K_α ray of Co ($\lambda = 0.179\,02$ nm).

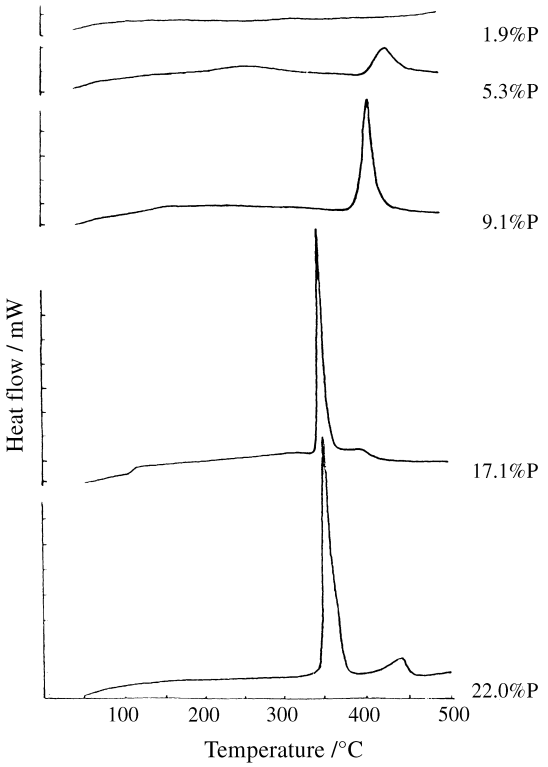

Fig. 5. Thermograms of Ni–P electrodeposits obtained from differential thermal analyses (DTA).

3.2. *Thermal Stability*

The metal–metalloid alloys are well known for their thermodynamic metastability [13, 14], but we have seen that, when electrodeposited, they may contain gaseous species that can desorb during heat treatment at elevated temperatures depending on the crystallization state. We have studied hydrogen thermodesorption during heat treatments of NiP alloys and have correlated the results obtained with differential thermal analysis and dilatometry results.

As can be seen in Fig. 5, the quantity of phosphorus in nickel solid solution modifies the slope of the thermogram so that two types of curve appear characteristic of the different processes occurring during heat treatment. In the composition range where the alloys are microcrystallized, there appears only one exothermic peak which, from examination of the X-ray diffraction patterns (Fig. 6), can be attributed to the crystallization of nickel phosphide Ni_3P from the nickel–phosphorus supersatured solid solution. For the amorphous alloys, the thermograms exhibit two exothermic peaks among whom the first at lower temperature, might correspond to precipitation of nickel phosphide phases increasingly richer in P (e.g.: Ni_3P, Ni_5P_2, and Ni_2P) with increasing phosphorus content in the deposits. The second transformation, appearing around 400 °C, may correspond to the coalescence of nickel phosphides and formation of stable phases of pure nickel and Ni_3P. The decrease in temperature from 400 to 360 °C of the crystallization onset with the phosphorus content in deposits show, as reported earlier [13], that the level of thermal instability of the nickel-phosphorus supersatured solid solution increases with the deposit metalloid content.

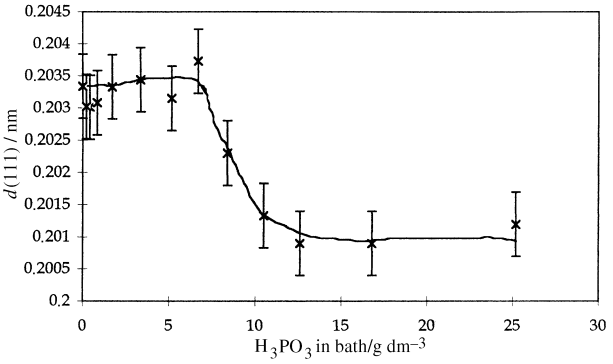

Fig. 4. Variation of the interreticular distance of (1 1 1) planes against phosphorus content in alloys.

From thermal expansion analyses, an anomalous expansion phenomenon was observed during heat treatment of alloys containing more than 9 at% of phosphorus (Fig. 7). It is well known that disordered solid solutions, like microcrystallized or amorphous Ni–P alloys, have a lower density than crystallized alloys with the same chemical composition [15], and the amorphous-crystallized transition is attended by a thermal contraction phenomenon [16]. In the case of microcrystallized or amorphous electrodeposited Ni–P alloys we have also observed (Fig. 8) that the amplitude of the phenomenon increases with the phosphorus content in the deposits. The increase in contraction amplitude and the decrease in the contraction onset temperature confirm the increase in metastability of these alloys when the phosphorus content is increased beyond 9 at%.

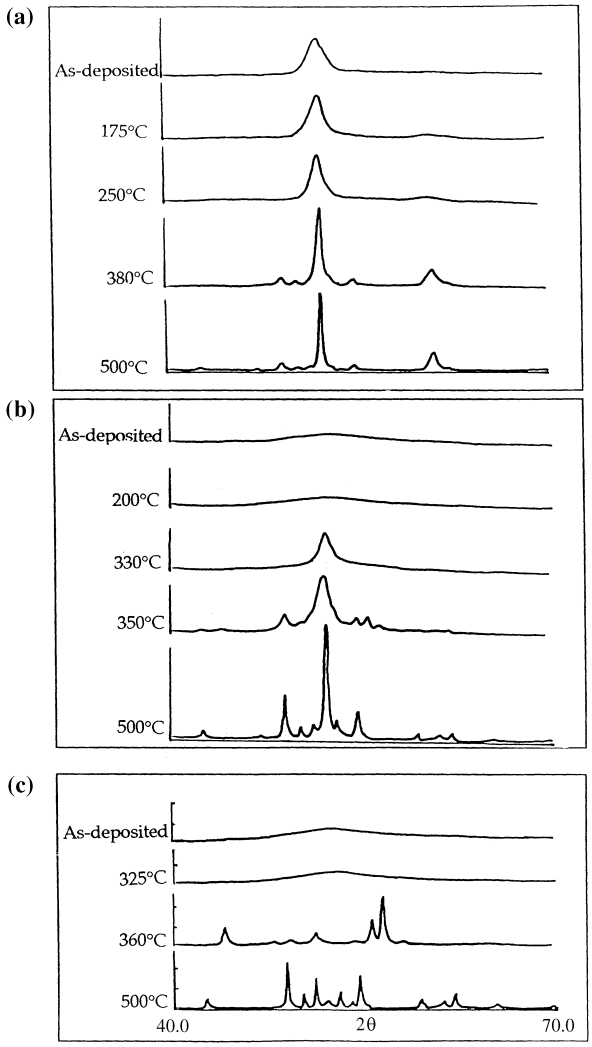

Fig. 6. X-ray diffraction patterns of annealed Ni–P electrodeposits: (a) 9.1 at%; (b) 17.9 at%; (c) 22 at% of phosphorus.

The thermodesorption curves reported on Fig. 9 show that the crystallization phenomena of electrodeposited amorphous alloys during heat treatment is not the only cause of densification. In fact, hydrogen desorption appears to occur in two steps. The first, from 100 to 300 °C, apparently corresponds to the hydrogen desorbed from the Ni–P solid solution without structural modification. The second, beyond 350 °C, appears during crystallization of nickel phosphides Ni_3P. The desorption begins at 100 °C for each alloy, but we observed more than once that

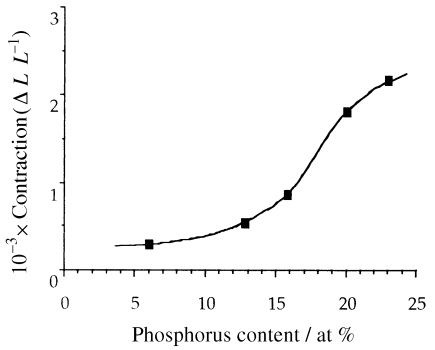

Fig. 8. Variation of contraction amplitude characteristic to the anomalous thermal expansion of Ni–P against the phosphorus content in deposits.

these alloys can be separated into two composition ranges according to their thermodesorption curves. Figure 10 reports the variation of hydrogen desorbed as a function of the phosphorus content in the deposits. For the (1 0 0)-oriented microcrystallized alloys containing less than 9 at% phosphorus, the quantity of hydrogen desorbed is very low but increases with P content until the (2 0 0) peak disappears (Fig. 2). From deposits containing more than 9 at% of phosphorus, the hydrogen desorbed during the first desorption increases rapidly from 20 $cm^3\ g^{-1}$ to 80 $cm^3\ g^{-1}$ as the phosphorus content increases from 9 to 17 at%. These results are in good agreement with the decrease in current efficiency and the increase in lattice distortion described above, and confirm the high hydrogen content in this family of deposits. Since the first hydrogen desorption occurs at temperatures below the crystallization temperature, the thermal contraction phenomenon appearing during heat treatment of alloys containing more than 9 at% phosphorus cannot be attributed solely to crystallization of denser phases during the amorphous-crystalline transition.

4. Conclusion

Under given experimental conditions, increased phosphorus codeposition resulting from increased H_3PO_3 concentration in the bath, apparently produces a change in the nickel electrodeposition mechanism. Up to 7 $g\,dm^{-3}$ H_3PO_3 in the bath, microstructural refinement is attended by a change in

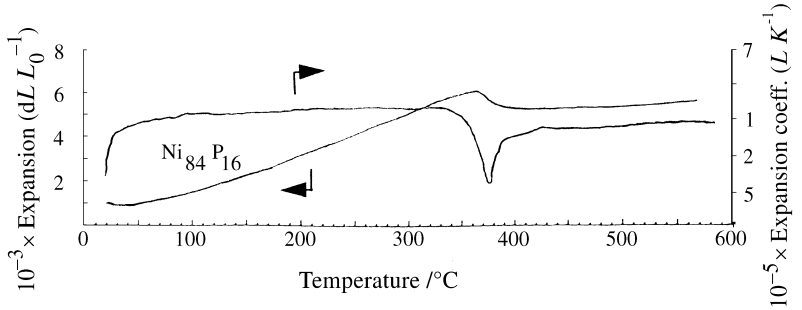

Fig. 7. Thermal expansion behaviour of $Ni_{84}P_{16}$ electrodeposits.

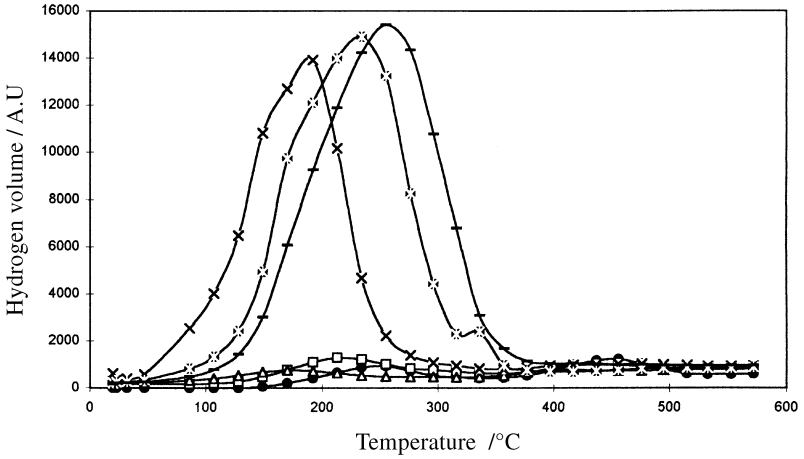

Fig. 9. Thermal desorption properties of Ni–P electrodeposits. Key: (●) $Ni_{98}P_2$; (□) $Ni_{95}P_5$; (Δ) $Ni_{91}P_9$; (×) $Ni_{82}P_{18}$; (☆) $Ni_{79}P_{21}$ and (–) $Ni_{78}P_{22}$.

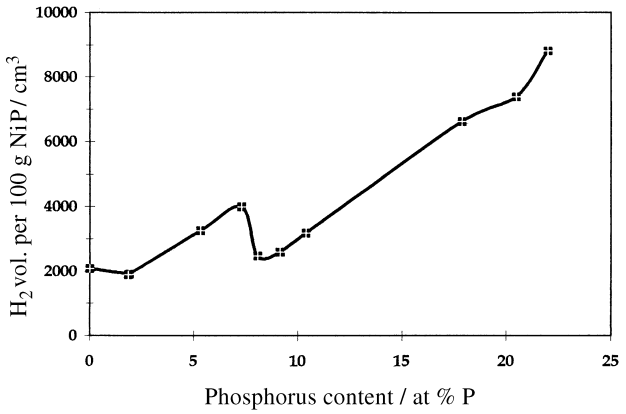

Fig. 10. Variation of hydrogen desorbed from Ni–P electrodeposits against phosphorus content.

crystallographic orientation of grains, from (100) to (1 1 1). Along this change of texture, we observe slight adsorption of hydrogen. Above 9 at % phosphorus in the deposit, the microcrystallized alloys gradually lose the (1 1 1) texture and become amorphous, and adsorb large volumes of hydrogen. Thermodesorption analysis show that most hydrogen desorption occurs before the crystallization temperature, and that a lesser quantity is desorbed during the crystallization.

References

[1] R. Narayan and M. N. Mungole, *Surf. Technol.* **24** (1985) 233.
[2] D. S. Lashmore and J. Weinroth, *Plat. & Surf. Finish.* **69** (8) (1982) 72.
[3] N. Feldstein and T. S. Lancsek, *J. Electrochem. Soc.* **137** (4) (1990) 1107.
[4] G. McMahon and U. Erb, *J. Mater. Sci. Lett.* **8** (1989) 865.
[5] A. Staudinger and S. Nakahara, *Thin Solid Films* **45** (1977) 125.
[6] J.-P. Bonino, P. Pouderoux, C. Rossignol and A. Rousset, *Plat. & Surf. Finish.* **79**, (4) (1992) 62.
[7] R. L. Zeller III and U. Landau, *J. Electrochem. Soc.* **13** (4) (1990) 1107.
[8] P. Pouderoux, PhD. Toulouse III University (1991), France.
[9] H. Maeda, *Trans. Nat. Res. Inst. Metals* **12** (1970) 211.
[10] E. Vafaei-Makhsoos, E. L. Thomas and L. E. Toth, *Metall. Trans. A*, **9** (1978) 1149.
[11] J. Amblard, I. Epelboin, M. Froment and G. Maurin, *J. Appl. Electrochem.* **9** (1979) 233.
[12] C. Kollia, N. Spyrellis, J. Amblard, M. Froment and G. Maurin, *J. Appl. Electrochem.* **80** (1990) 1025.
[13] P. Pouderoux, I. Chassaing, J.-P. Bonino and A. Rousset, *Surf. & Coat Technol.* **45** (1991) 161.
[14] M. L. Sui and K. Lu, *Mater. Sci. Engng.* **A179/A180** (1994) 541.
[15] F. E. Fujita, *Sci. Rep. Univ. Tohoku, Ser.* A, **28** (1980) 1.
[16] K. Lu, M. L. Sui and R. Lück, *Nanostruct. Mater.* **4** (1994) 645.